

NORSAR Scientific Report No. 2-90/91

Semiannual Technical Summary

1 October 1990 — 31 March 1991

Kjeller, May 1991

APPROVED FOR PUBLIC RELEASE, DISTRIBUTION UNLIMITED

7.5 A 2-dimensional finite difference approach to modeling seismic wave propagation in the crust

Introduction

It is well known that the direct, discrete solution of the elastic wave equation constitutes an excellent platform for synthetic seismogram analysis as *all* propagation effects are included in the solution (e.g., see Mooney, 1983). A practical realization of this approach has been problematic until recently due to limitations imposed by currently available computers. This being said, we will report below on 2-dimensional (2D) finite difference seismogram synthetic experiments which have been achieved through cooperative efforts with scientists at IBM Bergen Scientific Centre (Bergen, Norway).

Elastic wave modeling formulation

The basic equations governing wave propagation in a continuous elastic medium are the momentum conservation and the stress-strain relation. Following Achenbach (1975), in the velocity-stress formulation, these are given by

$$\rho \frac{\partial}{\partial t} v_j = f_j + \frac{\partial}{\partial x_\ell} \sigma_{j\ell}, \quad j, \ell = 1, \dots, J \quad (1)$$

$$\frac{\partial}{\partial t} \sigma_{jj} = \lambda \frac{\partial}{\partial x_\ell} v_\ell + 2\mu \frac{\partial}{\partial x_j} v_j, \quad j, \ell = 1, \dots, J \quad (2)$$

$$\frac{\partial}{\partial t} \sigma_{j\ell} = \mu \left(\frac{\partial}{\partial x_j} v_\ell + \frac{\partial}{\partial x_\ell} v_j \right), \quad j, \ell = 1, \dots, J, \quad j \neq \ell \quad (3)$$

where Einstein's summation convention is used. J is the dimensionality of the problem, ρ is density, and λ and μ are Lamé's parameters. f_j are body forces and v_j and $\sigma_{j\ell}$ are velocities and stresses, respectively.

Numerical discretization

Spatial partial differentiation is achieved through cost-optimized, dispersion-bounded, high-order finite difference operators on a staggered grid. For time stepping a leap-frog technique is used. The discretization of the elastodynamic equations with two staggered numerical space differentiators, σ^\pm , applied as in Levander (1988) to stresses and particle velocities leads to:

$$\rho_j^+ \{V_j^+(t + \Delta t/2) - V_j^+(t - \Delta t/2)\} = \Delta t \{F_j^+(t) + \delta_j^+ S_{jj}(t) + \sum_{\substack{l=1 \\ l \neq j}}^J \delta_l^- S_{jl}^{++}(t)\}, \quad j, l = 1, \dots, J$$

$$S_{jj}(t + \Delta t) - S_{jj}(t) = \lambda \Delta t \sum_{r=1}^J \delta_r^- V_r^+(t + \Delta t/2) + 2\mu \Delta t \delta_j^- V_j^+(t + \Delta t/2), \quad j, l = 1, \dots, J$$

$$S_{jl}^{++}(t + \Delta t) - S_{jl}^{++}(t) = \mu_{jl}^{++} \Delta t \{\delta_j^+ V_l^+(t) + \delta_l^+ V_j^+(t)\}, \quad j, l = 1, \dots, J, \quad j \neq l$$

with

$$V_j^+(t) = v_j(\mathbf{x} + \mathbf{h}_j/2, t), \quad F_j^+(t) = f_j(\mathbf{x} + \mathbf{h}_j/2, t),$$

$$S_{jj}(t) = \sigma_{jj}(\mathbf{x}, t), \quad S_{j_l}^{++}(t) = \sigma_{j_l}(\mathbf{x} + \mathbf{h}_j/2 + \mathbf{h}_l/2, t),$$

$$\rho_j^+ = \rho(\mathbf{x} + \mathbf{h}_j/2), \quad \lambda = \lambda(\mathbf{x}), \quad \mu = \mu(\mathbf{x}) \quad \text{and} \quad \mu_{j_l}^{++} = \mu(\mathbf{x} + \mathbf{h}_j/2 + \mathbf{h}_l/2).$$

$$\delta_j^+ q(\mathbf{x}) = \sum_{\ell=1}^{L^+/2} d_{2\ell-1}^+ \frac{q(\mathbf{x} + \ell \mathbf{h}_j) - q(\mathbf{x} - (\ell-1) \mathbf{h}_j)}{\Delta x_j} \cong \frac{\partial q}{\partial x_j}(\mathbf{x} + \mathbf{h}_j/2),$$

$$\delta_j^- q(\mathbf{x}) = \sum_{\ell=1}^{L^-/2} d_{2\ell-1}^- \frac{q(\mathbf{x} + (\ell-1) \mathbf{h}_j) - q(\mathbf{x} - \ell \mathbf{h}_j)}{\Delta x_j} \cong \frac{\partial q}{\partial x_j}(\mathbf{x} - \mathbf{h}_j/2).$$

Here \mathbf{h}_j is the unit vector in the j th direction, λ , μ and S_{ij} are defined at the nodes of the Cartesian mesh, ρ_j^+ , V_j^+ and F_j^+ are defined at the links connecting the nodes and $S_{j\ell}^{++}$ and $\mu_{j\ell}^{++}$ are defined at the centers of the "plaquettes". σ^\pm are numerical differentiators of coefficients $d_{2\ell-1}^\pm$. q is here velocity or stress and L^\pm is the length of the operator. For the numerical dispersion relations, the stability limit and bandwidth introduced by the discretization, the reader is referred to Sguazzero *et al* (1990).

Absorbing and free surface boundary conditions

By necessity, the numerical modeling limits the medium, and to reduce artificial reflections from the numerical boundaries, the velocities and stresses are multiplied by exponentially decreasing terms near the edges. For this procedure to be efficient, relatively large models are required, that is, relatively large spatial distances to the wedges and this in 3D modeling would be computationally very demanding. In the latter case we have experimented with boundary operators recently introduced by Higdon (1990,1991), which at $x = 0$ read like

$$\prod_{j=1}^m \left(\cos \alpha_j \frac{\partial}{\partial t} - c_j \frac{\partial}{\partial x} \right)$$

which will absorb perfectly a plane wave travelling towards the boundary at angle

α_j and speed c_j . m is the order of the operator. Similar operators are used on the other boundaries. The condition for this method to be useful is that the number of time steps is small enough not to exceed a certain limit, after which the method will appear unstable.

On the top free surface, we use the vanishing stress conditions for a free boundary

$$\vec{n} \cdot \mathbf{T} = 0 \quad (4)$$

Here \vec{n} is the outward normal unit vector on the surface and \mathbf{T} is the stress tensor. To get computationally tractable conditions, we assume the free top surface to be locally plane. Then $\vec{n} = \vec{k}$, where \vec{k} is the unit vector in the vertical z -direction. x and y are horizontal coordinates. (4) then leads to

$$\sigma_{zx} = \sigma_{zy} = \sigma_{zz} = 0 \quad (5)$$

To increase the generality, one may assume a topographic relief as the free surface. By relaxing the requirement of the surface being locally plane, one assumes a given slope locally in each spatial direction. The resulting conditions on the stresses become more complex, though tractable, as demonstrated by Jih *et al* (1988).

At present we have not incorporated the “topography” free surface in our software.

Crustal wave propagation — 2D finite difference synthetics

The task of “adapting” the 2D FD software for handling of seismological problems has been rather time consuming. Hence, only recently have we been able to produce seismic synthetics for crustal wave propagation. We can also handle 3D cases, but their seismological relevance at present is limited. Anyway, in the following we will present some examples of synthetic seismograms.

Model description and data analysis

Basically we use a homogeneous crust of thickness 30 km and $P_{vel} = 6.5$ km/sec, which besides serves as a reference model. The options for perturbing this model comprise multilayering, piecewise linear velocity gradients, large-scale discontinuities like Moho bump(s), but so far no randomized scatter inclusions. A schematic model illustration is shown in Fig. 7.5.1. Although the source (point or line source) could be at any depth, the sensors are always on the free surface. Any sensor configuration could be used, although our performance is for a 10-element line array with 0.4 km sensor interspacing, which is convenient for velocity decomposition of the synthetics. Occasionally we use a sensor spacing of 5 km in order to visualize the distance variability in the records.

An objection against 2D solutions of the elastic wave equation is that all propagation effects are included and hence it would be difficult to isolate the response

of a specific body within the synthetic wavetrain. To overcome this kind of problems, we would process the synthetic records in a manner similar to that used for real recordings. Principal techniques used are frequency wavenumber (f-k), semblance and 3-component polarization analysis (e.g., see Husebye and Ruud, 1989). Occasionally we would make comparisons with "ray tracing" synthetics for which more specific contribution effects are specified *a priori*.

Results

Examples of crustal synthetics using the procedure outlined above are shown in Figs. 7.5.2, 7.5.3 and 7.5.4. The following comments apply.

Figs. 7.5.2 and 7.5.3: Bump on Moho — ranges 160 km and 210 km

In Figs. 7.5.2b and 7.5.3b the homogeneous cases are shown, while the bump cases are shown in Figs. 7.5.2a and 7.5.3a, respectively. A comparison here gives that the Moho bump does not strongly change the records, which is also rather obvious from a corresponding comparison of the semblance plots in Figs. 7.5.2c,d and Fig. 7.5.3c,d, respectively. The dominant features in the synthetics appear to be crustal reverberations (PmP), which are particularly abundant since the signal source was put at a depth of 10 km.

Fig. 7.5.4: Bump on Moho — ranges 100–200 km

In this case, we used a linear velocity gradient in the crust and besides used a sensor spacing of 5 km in order to visualize distance-dependent changes in the records. As observed, the Pg-phase dominates the first part of the records, then comes the corresponding S-phases and finally multimode Rayleigh-type of waves. With the much larger sensor spacing the semblance resolution is very high, as illustrated in Fig. 7.5.4c,d. We have also tested the signal polarity, which further adds weight to the realism of the 2D FD synthetics displayed.

Discussion and future work

The synthetics generated seemingly include *all* major phases, while in comparison to real records the body wave coda is weak to nonexistent. As demonstrated, long wavelength heterogeneities like a bump on Moho do not contribute much in this respect. This in turn implies that the cumulative propagation effect of randomly distributed scatterers are likely to be of importance.

A specific advantage with our technique for 2D synthetic seismogram calculations is flexibility in choosing model parameters. In our future work, some sort of a reference crustal model would be established. Then we would systematically change the velocity structure both above and below Moho. Scatterers would be introduced at various parts of the travel path, and their effect would be visualized partly but taking the difference between "homogeneous" and "inhomogeneous" synthetics. Finally, we would naturally compute synthetics on the basis of crustal

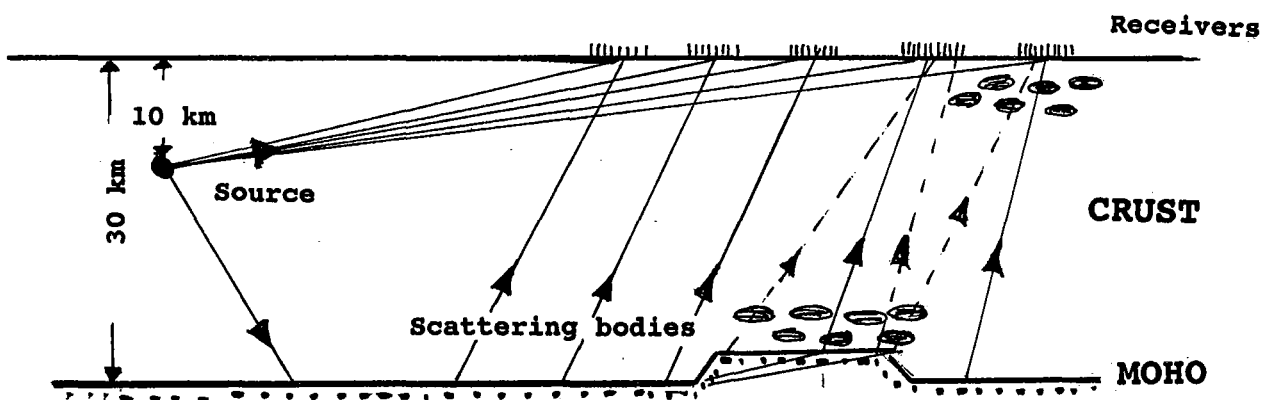
results presented in Section 7.6.

S. Hestholm, IBM Bergen Sci. Centre
B. Rosland, IBM Bergen Sci. Centre
B.O. Ruud, Geol. Inst., Univ. of Oslo
E.S. Husebye

References

- Achenbach, J.D. (1975): *Wave Propagation in Elastic Solids*, North Holland Publ. Co., The Netherlands.
- Higdon, R.L. (1990): Radiation boundary conditions for elastic wave propagation, *SIAM J. Num. Anal.*, April.
- Higdon, R.L. (1991): Absorbing boundary conditions for elastic waves, *Geophysics*, to appear.
- Husebye, E.S. and B.O. Ruud (1989): Array seismology — Past, present and future developments, in *Observatory Seismology*, J.J. Litehiser, Ed., Berkeley Univ. Press, Berkeley, California, 123–153.
- Jih, R.-S., K.L. McLaughlin and Z.A. Der (1988): Free boundary conditions of arbitrary polygonal topography in a two-dimensional explicit elastic finite-difference scheme, *Geophysics*, 53, 1045–1055.
- Levander, A.R. (1988): Fourth-order finite-difference P-SV seismograms, *Geophysics*, 53, 1425–1436.
- Mooney, H.M. (1983): Synthetic seismograms for body waves: An overview, *First Break*, dec, 9-20.
- Sguazzero, P., M. Kindelan and A. Kamel (1990): Dispersion-bounded numerical integration of the Elastodynamic equations, *Comp. Meth. Appl. Mech. Eng.*, 18.

2D ELASTIC MODELLING - OSLO RIFT



PROCESSING: F-K; SEMBLANCE AND 3C ANALYSIS

OBSERVATION: NORESS ARRAY RECORDINGS

Fig. 7.5.1. Simple one-layered crustal model used initially for computing synthetic seismograms based on finite difference solutions in 2-dimensional (2D) of the elastic wave equations. The point source is located at a depth of 10 km; crustal and sub-Moho velocities are 6.5 km/sec and 8.2 km/sec, respectively. Corresponding density values are 2.85 kg/m³ and 3.34 kg/m³. The Moho bump is 50 m wide and 2 or 4 km high. Horizontal distance from source to nearest edge of Moho bump is 100 km. So far scatter inclusions with contrasts in velocity and density of the order of 2-5 per cent have not been included.

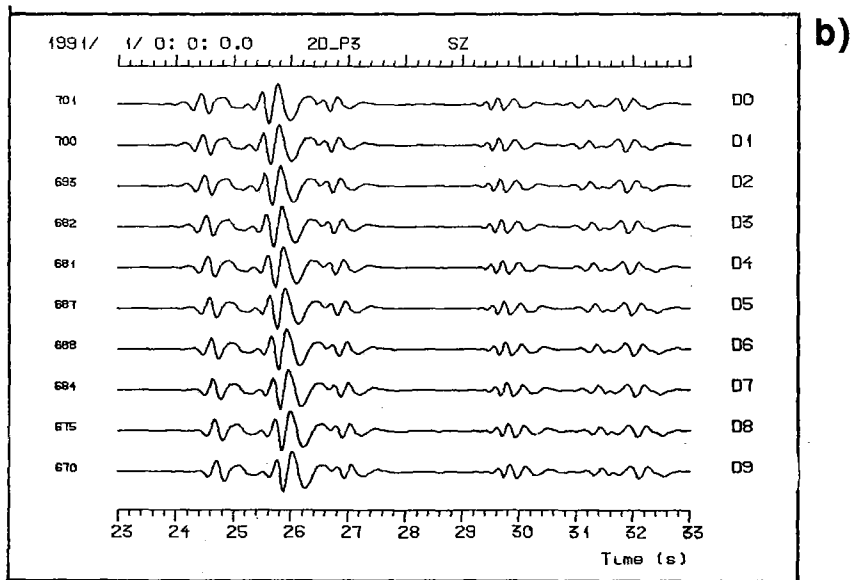
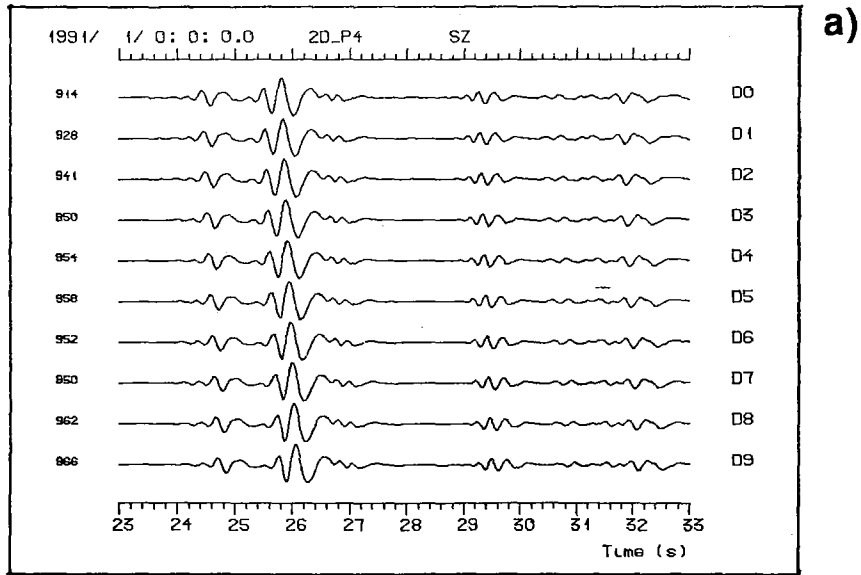


Fig. 7.5.2a and b. 2D FD synthetics for the model shown in Fig. 7.5.1. In figure b, the Moho bump of 2 km has been removed. The horizontal distance from source to the nearest sensor is 160 km while sensor interspacing is 200 m.

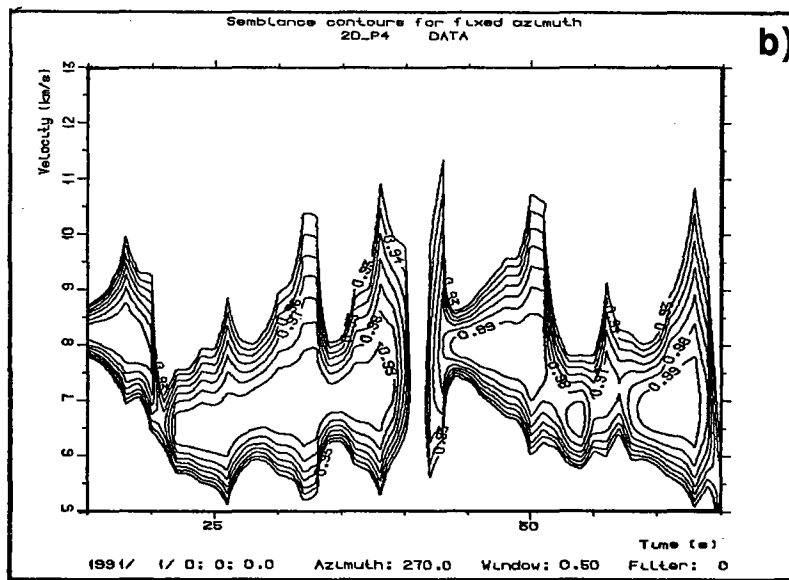
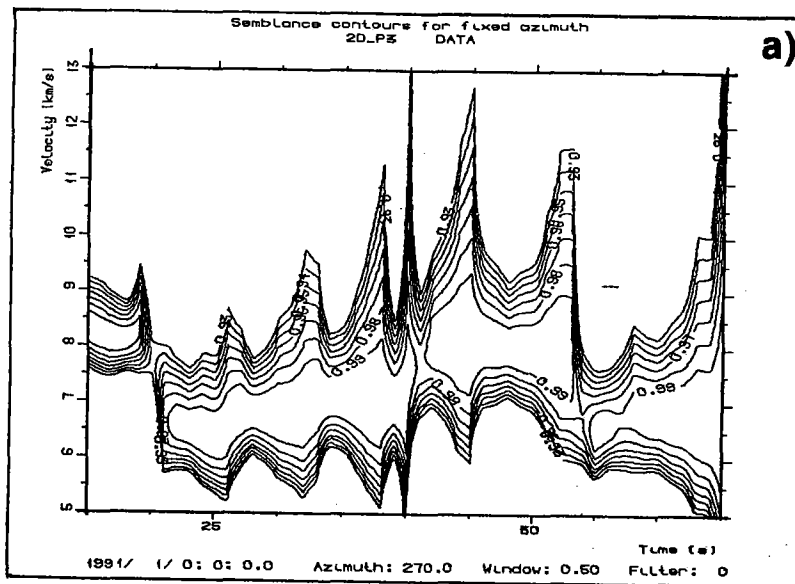


Fig. 7.5.3a and b. Semblance velocity (VESPAGRAM) analysis of the synthetics displayed in Fig. 7.5.2a and b, respectively. Seemingly the effect of a bumpy Moho is marginal. Also, "ray paths" within the crust and sub-Moho are easily identified from this velocity plot.

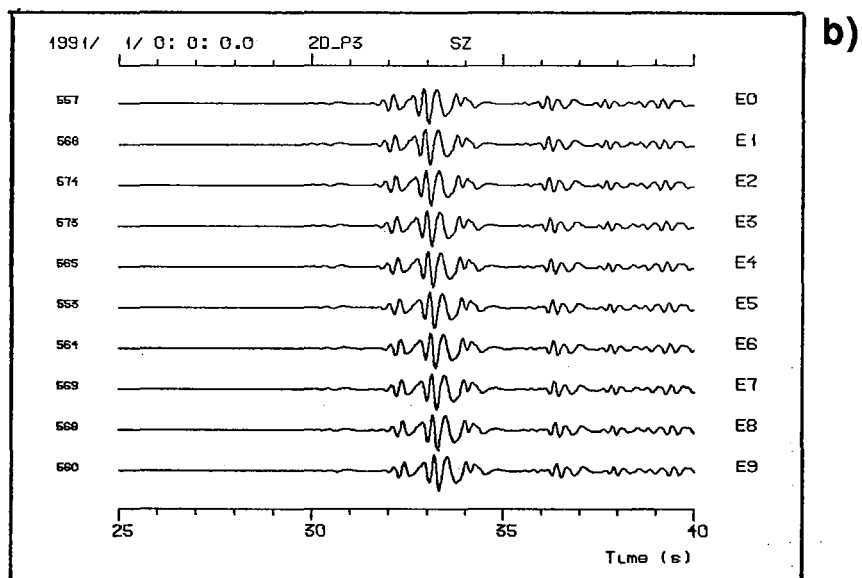
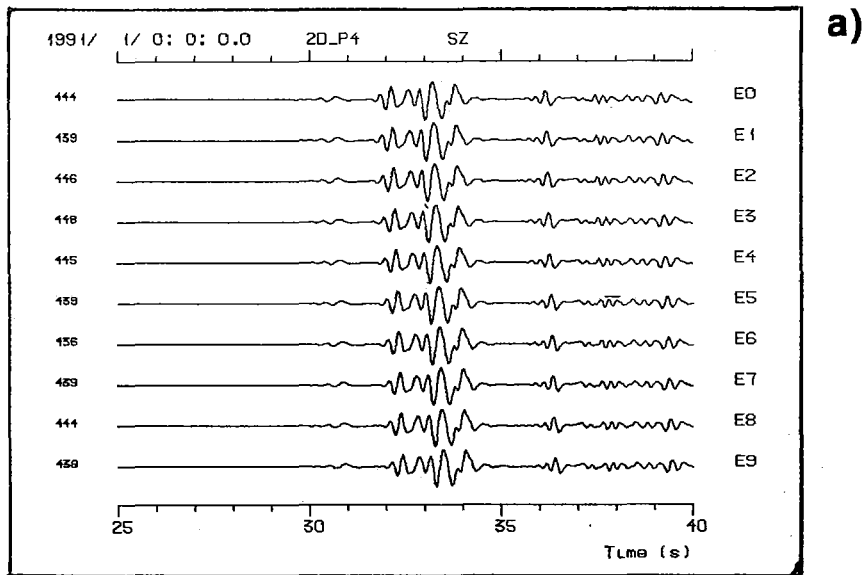


Fig. 7.5.4a and b. Same as for Fig. 7.5.2, but now the horizontal distance to the nearest sensor is 210 km.

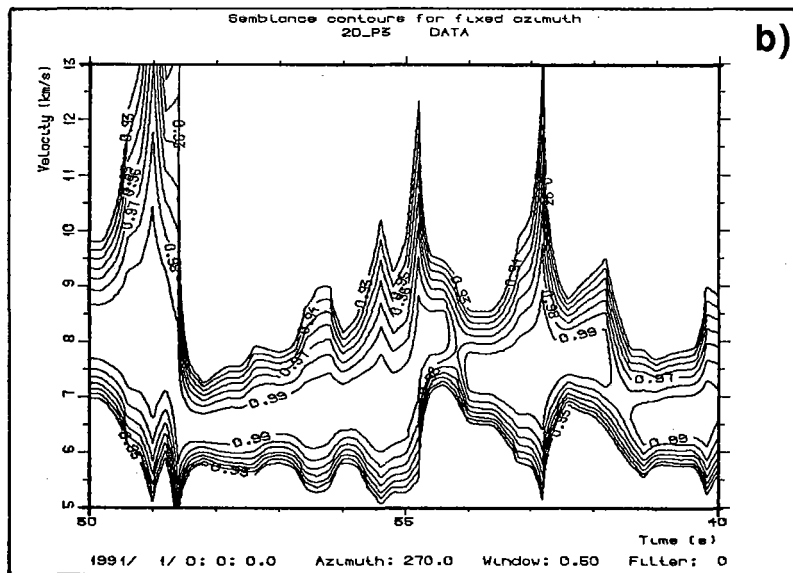
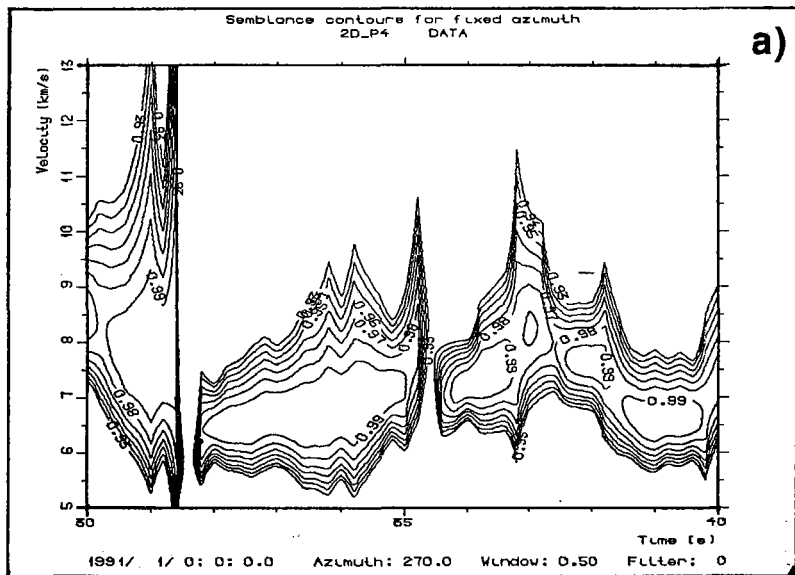


Fig. 7.5.5a and b. Semblance velocity (VESPAGRAM) analysis for the synthetics shown in Fig. 7.5.4.

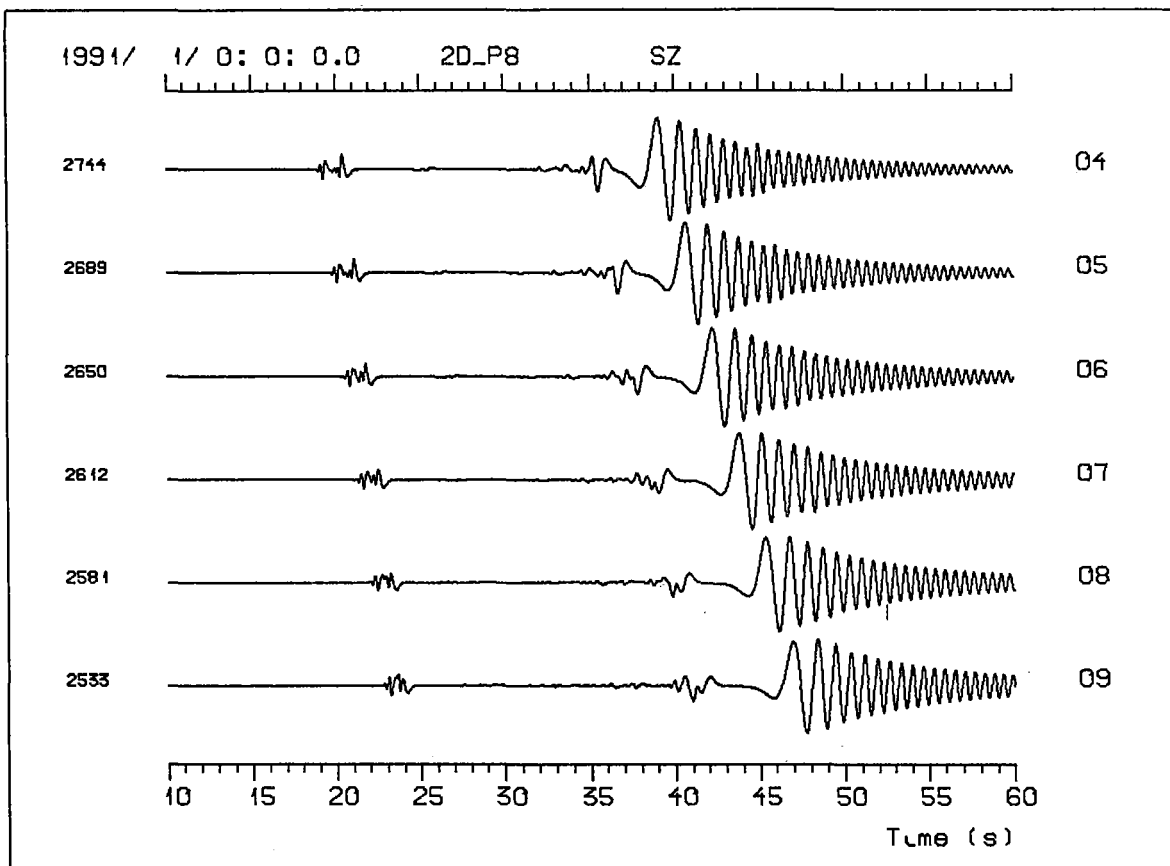


Fig. 7.5.6a. Crustal 2D FD synthetics of 60 sec duration. In this case the point source is just below the surface and the P-velocity increases linearly from 6.2 to 7.0 km/sec at the bottom of the crust. Below Moho the P-velocity increases linearly from 8.2 to 8.4 km/sec from 30 to 40 km. Below 40 km the velocity is fixed at 8.4 km/sec. Distance range is 115–140 km with a 5 km interspacing of sensors.

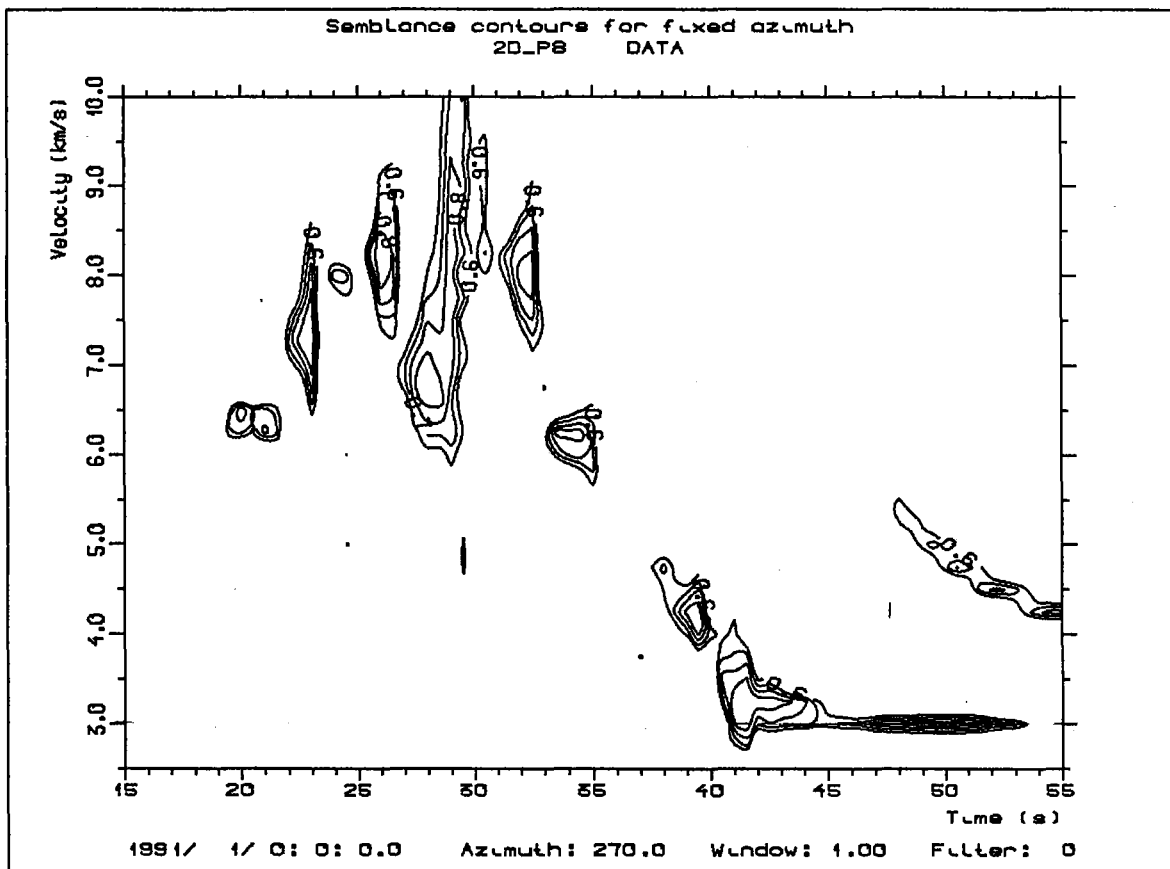


Fig. 7.5.6b. Semblance velocity (VESPAGRAM) analysis of the synthetics displayed in Fig. 7.5.6a. The first part of the synthetics is dominated by crustal reverberations (phase velocities above 8.0 km/sec hardly seen). The Pg-phase around 35 sec preceding the S-wave at around 39 sec is a commonly observed feature. Dispersive Rayleigh waves are also synthesized. Time reference is tied to sensor 06.